

A Modeling Study of the Satilla River Estuary, Georgia. II: Suspended Sediment

LIANYUAN ZHENG¹, CHANGSHENG CHEN^{2,*}, MERRYL ALBER³, and HEDONG LIU²

¹ College of Marine Science, University of South Florida, St. Petersburg, Florida 33701

² School for Marine Sciences and Technology, University of Massachusetts-Dartmouth, New Bedford, Massachusetts 02742

³ Department of Marine Sciences, University of Georgia, Athens, Georgia 30602

ABSTRACT: A three-dimensional (3-D) suspended sediment model was coupled with a 3-D hydrodynamic numerical model and used to examine the spatial and temporal distribution of suspended sediments in the Satilla River estuary of Georgia. The hydrodynamic model was a modified ECOM-si model with inclusion of the flooding-drying cycle over intertidal salt marshes. The suspended sediment model consisted of a simple passive tracer equation with inclusion of sinking, resuspension, and sedimentation processes. The coupled model was driven by tidal forcing at the open boundary over the inner shelf of the South Atlantic Bight and real-time river discharge at the upstream end of the estuary, with a uniform initial distribution of total suspended sediment (TSS). The initial conditions for salinity were specified using observations taken along the estuary. The coupled model provided a reasonable simulation of both the spatial and temporal distributions of observed TSS concentration. Model-predicted TSS concentrations varied over a tidal cycle; they were highest at maximum flood and ebb tidal phases and lowest at slack tides. Model-guided process studies suggest that the spatial distribution of TSS concentration in the Satilla River estuary is controlled by a complex nonlinear physical process associated with the convergence and divergence of residual flow, a non-uniform along-estuary distribution of bottom stress, and the inertial effects of a curved shoreline.

Introduction

Georgia's Satilla River has a well-mixed estuary with a mean water depth of about 4 m and a maximum tidal current of about 140 cm s^{-1} (Blanton et al. 1999; Zheng et al. 2003). Tidally induced residual currents are characterized by multiple eddy-like convergences and divergences. The maximum subtidal velocity is over 15 cm s^{-1} and occurs where the shoreline has a significant bend. This complex three-dimensional (3-D) residual current feature is predominately driven by tidal mixing, asymmetry of the tidal current, the along-river baroclinic pressure gradient, and centrifugal forcing associated with the curved shoreline (Zheng et al. 2003). Strong tidal currents in such a shallow estuary cause energetic vertical turbulent mixing and tidal mixing is generally stronger during the flood tide than during the ebb tide (Dronkers 1986). The freshwater discharge of the river varies seasonally, with a 30-yr median value of $34 \text{ m}^3 \text{ s}^{-1}$ and an annual maximum flow of about $1,000 \text{ m}^3 \text{ s}^{-1}$ during the spring. Buoyancy-induced flow tends to accelerate the offshore advection during ebb tide but slows down the landward movement during flood tide, causing an asymmetrical current pattern over the course of a tidal cycle. The residual circulation

pattern is intensified significantly and shifted downstream when freshwater discharged is included. In addition, the Satilla River estuary is bounded by shorelines that feature complex curvature. The cross-estuary residual current is generally stronger near the curved river shoreline, which is a result of the imbalance between the centripetal and cross-estuary pressure gradients (Fischer et al. 1979; Geyer 1993; Ridd et al. 1998).

One of the most important features of the Satilla River estuary is the existence of extensive intertidal salt marshes. These marshes are completely flushed at slack high water and remain dry at slack low water. They act like a water-absorber that directly accelerates water movement inside the estuary over a tidal cycle. This can be seen in tidal simulations using a fully 3-D primitive-equations model (Zheng et al. 2003), which shows that tidal currents in the main channel of the estuary can be increased 40–50% when the flooding-drying cycle over the intertidal salt marshes is included. The flooding-drying process over intertidal salt marshes also tends to enhance the asymmetry of tidal currents over a tidal cycle, resulting in a relatively large residual flow along the estuary. The importance of tidal asymmetry in transport and accumulation of sediment in an estuary has been well documented (Fitzgerald and Nummedal 1983),

* Corresponding author; e-mail: clchen@umassd.edu.

and we were interested in extending our hydrodynamic model to examine sediment dynamics.

A comprehensive interdisciplinary survey was conducted in the Satilla River estuary during spring tide in April 1995. Optical backscatter measurements at slack high water revealed a non-uniform spatial distribution of total suspended sediment (TSS) concentration along the estuary transect (Blanton et al. 1999) with two maximum TSS concentrations exceeding 150 mg l^{-1} near the bottom: one 13 km upstream from the mouth of the estuary where the shoreline has a significant concave bend and the other near the estuary mouth (see Fig. 1a in Zheng et al. 2003). At an anchor site, a distance of 16 km from the mouth of the estuary, the TSS concentrations varied considerably over a tidal cycle. They were highest at maximum flood and ebb tides and lowest at slack high and low tides (see Fig. 1b in Zheng et al. 2003). Maximum TSS concentration occurred about 1.5 h after maximum ebb current and 2 h after maximum flood current (Blanton et al. 1999). Around maximum ebb tide, TSS concentrations exceeding $1,000 \text{ mg l}^{-1}$ were found throughout the water column. Around maximum flood tide, TSS concentrations exceeding $1,000 \text{ mg l}^{-1}$ were trapped near the bottom and decreased toward the surface. At slack low water, TSS concentration near the surface was more than 100 mg l^{-1} . At slack high water, however, it was trapped near the bottom and the near-surface concentration was only about 20 mg l^{-1} .

What are the physical processes that cause the non-uniform spatial distribution and asymmetrical temporal variation of TSS concentration in the Satilla River estuary? Generally speaking, the distribution of TSS in an estuary is controlled by complex nonlinear processes associated with the interaction between wind-induced waves, asymmetrical tidal horizontal advection and vertical mixing, short-term and long-term variations in estuarine circulation, stratification, bottom stress (resuspension), particle settling velocity (deposition), and flocculation-deflocculation processes (Postma 1967; Dyer 1986; Sanford et al. 1991; Geyer 1993; Uncles and Stephens 1993; Jay and Musiak 1994; Lou and Ridd 1997). Which of these processes is dominant in the Satilla River estuary? To our knowledge, this question has not been addressed in previous modeling studies in that area.

We used a coupled 3-D hydrodynamic and suspended sediment model to examine the physical processes that control the non-uniform spatial distribution of TSS concentration in the Satilla River estuary. This coupled model was developed based on a 3-D hydrodynamic model of the Satilla River estuary with inclusion of numerical treatment for the flooding-drying cycle over the intertidal salt

marshes (Zheng et al. 2003). The suspended sediment model consists of a 3-D passive tracer equation with inclusion of sinking, resuspension, and sedimentation processes (Ariathurai and Krone 1976). We used the model to perform a retrospective simulation of the observations of April 1995 described above. This simulation helped us verify that the model captured the basic spatial and temporal distribution patterns of the observed TSS in the Satilla River estuary. A series of process studies was also carried out to explore the physical driving mechanisms responsible for the observed distribution of TSS.

Suspended Sediment Model

The TSS model used in this study is a 3-D simple passive tracer equation with inclusion of sinking, sedimentation, and resuspension processes. Ignoring the feedback effects of TSS on fluid motion as well as on flocculation and deflocculation processes, the TSS concentration in the water column can be estimated by a concentration equation as follows:

$$\begin{aligned} \frac{\partial C}{\partial t} + \frac{\partial uC}{\partial x} + \frac{\partial vC}{\partial y} + \frac{\partial (w - w_s)C}{\partial z} \\ = \frac{\partial}{\partial z} \left(K_h \frac{\partial C}{\partial z} \right) + F_c \end{aligned} \quad (1)$$

where C denotes the suspended sediment concentration, u , v , and w are the x , y , and z components of the fluid velocity, K_h is the vertical eddy diffusivity, w_s is the settling velocity of suspended sediment, and F_c represents horizontal diffusion processes. The vertical eddy diffusivity K_h is determined by the turbulence intensity estimated from Mellor and Yamada's (1982) level 2.5 turbulent closure scheme.

The surface boundary condition for C is specified as no sediment flux, i.e.,

$$w_s C + K_h \frac{\partial C}{\partial z} = 0, \quad \text{at } z = \zeta(x, y, t) \quad (2)$$

where ζ is surface elevation. At the bottom, sediment flux is specified as the difference between resuspension and sedimentation, so that

$$-w_s C - K_h \frac{\partial C}{\partial z} = F_e - F_s, \quad \text{at } z = -H(x, y) \quad (3)$$

where

$$F_e = \begin{cases} \frac{c_e}{\rho_0} (|\tau_b| - \tau_{ce})^+ & \text{for } B > 0 \\ 0 & \text{elsewhere} \end{cases} \quad \text{and} \quad (4)$$

TABLE 1. Parameters of suspended sediments used in the model in the Satilla River estuary. w_s is settling velocity of the sediment and τ_{ce} is critical stress for resuspension.

Sediment Type	w_s (cm s ⁻¹)	τ_{ce} (kg s ⁻¹ m ⁻²)
Sand	2.81	0.196 ^a
Settleable	8.8×10^{-1b}	0.196 ^b
Nonsettleable	2.0×10^{-2c}	0.25×10^{-3c}

^a Middleton (1976); ^b Blake et al. (2001); ^c Alexander (unpublished data).

$$F_s = \frac{w_s C_b}{\tau_{cs}} (\tau_{cs} - |\tau_b|)^+ \quad (5)$$

F_e and F_s are the suspended sediment fluxes near the bottom caused by resuspension and sedimentation, respectively, c_e is a proportionality factor (constant value of 0.5), C_b is near-bottom suspended sediment concentration, τ_b is bottom shear stress, τ_{ce} is critical shear stress for resuspension, and τ_{cs} is critical shear stress for sedimentation. In this study, τ_{cs} is given the same value as τ_{ce} . The superscript ⁺ is an indicator of Heaviside's operator. B is the bottom suspended sediment pool, which is refilled by sedimentation and emptied by resuspension as

$$\frac{\partial B}{\partial t} = F_s - F_e \quad (6)$$

The resuspension of bottom sediment only occurs when both the bottom shear stress is larger than critical shear stress for resuspension and the bottom pool of sediment is available. With no flocculation and deflocculation processes, the interaction between different sizes of sediments can be neglected. This assumption allows us to divide the TSS into three individual groups: sand, settleable particles (silt and flocs), and nonsettleable (clay and small particles) particles (Table 1), and calculate their concentrations separately. The model-predicted TSS concentration is equal to a sum of the concentrations of sand, settleable, and nonsettleable particles. The critical shear stresses for resuspension and sedimentation of the three types of sediment shown in Table 1 are determined based on literature values (Middleton 1976; Blake et al. 2001) and unpublished data (Alexander personal communication).

To simplify our modeling experiments, two additional assumptions were made. No feedback effects of suspended sediment on water density were considered, which allowed us to easily couple the sediment model with the hydrodynamic model without modifying estuarine circulation and water density. The processes of sinking, resuspension, and sedimentation of particles over the intertidal salt marsh area were also not taken into account. This assumption was made based on mass conser-

vation, by which the inflow and outflow of the suspended sediment over salt marshes should be balanced in a climatologically averaged sense. Direct model-data comparisons under this simplification helped us identify and quantify the importance of intertidal salt marshes on TSS concentrations in the Satilla River estuary.

To examine how physical processes affect the spatial and temporal variation of TSS concentration, we assumed that suspended sediment concentration was initially uniformly distributed throughout the computational domain. This simplification made it easy to test the hypothesis that the spatial and temporal distributions of TSS were caused by physical processes associated with estuarine circulation, tidal mixing, and mixing between fresh and oceanic water. In the Satilla River estuary, observations revealed that the TSS mainly consisted of sand, settleable, and nonsettleable sediments (Alexander personal communication). The average size of a grain of sand is about 177 μm and its settling velocity is 2.81 cm s⁻¹ (Middleton 1976). Because sand sinks at a fast rate (it takes only 3–5 min to sink from surface to bottom given a mean depth of 5 m), it is generally trapped near the bottom. Its spatial and temporal distribution should be most affected by asymmetric tidal currents and stresses near the bottom. Settleable particles, such as flocs, are about 200 μm in size and have a settling velocity of 0.88 cm s⁻¹ (Blake et al. 2001). The settling time scale for this kind of sediment in 5 m of water is only about 10–15 min, which is much shorter than the tidal cycle. This type of sediment would also be trapped in the lower water column with a similar spatial distribution as the sand. The nonsettleable particles are very small and their settling velocity was specified as 0.02 cm s⁻¹ in the model (Alexander unpublished data). Since the settling time scale of these sediments in 5 m of water is approximately 7 h, which is slightly longer than half of a cycle of the semi-diurnal tide, they should be influenced significantly by asymmetric tidal advection and mixing and vertical stratification (Geyer 1993). Our numerical experiment started at neap tide slack low water on April 7, 1995. Given the fast settling velocities and large critical stresses for resuspension of sand and settleable particles (Table 1), we assumed that these particles would be found near the bottom at slack low water. The initial carbon (C) values were specified as zero for these two fractions. Several numerical experiments were conducted to test the sensitivity of the model-predicted distribution of sediments to the initial conditions, and no significant differences were found between sand and settleable particles. Observations conducted in the Satilla River indicated that the average concentration of the

nonsettleable particles was 15 mg l^{-1} in the upper 1 m below the surface and 45 mg l^{-1} in the lower 1 m above the bottom during neap tide (Alexander unpublished data). The initial C value of the nonsettleable particles was specified as 15 mg l^{-1} , the value observed near the surface.

One important parameter in the suspended sediment model is the bottom sediment pool, because its availability directly controls resuspension (i.e., when the bottom sediment pool approaches zero, bottom sediment resuspension will not occur even when bottom shear stress is larger than the critical shear stress for resuspension). Observations in the Satilla River estuary in April 1995 showed that bottom sediments were spatially variable throughout the estuary. In the region between 6 and 10 km from the estuary mouth, the bottom sediment was dominated by sand. In the rest of the region, however, it was dominated by settleable particles (Alexander unpublished data). On average, 30% of the material was sand and the rest was settleable particles (Alexander personal communication). To simplify, we specified initial bottom sediment pools for the three sediments' fractions as constant values over the entire computational domain. This specification is consistent with our objective, which was to determine the extent to which the observed spatial variations in suspended sediment concentration in the Satilla River estuary are caused by physical processes associated with tidal motion. The total concentration of sand and settleable particles near the bottom after the maximum current during spring tide was observed to exceed $6,000 \text{ mg l}^{-1}$ in the field measurement. This is 60 times larger than the maximum concentration observed in the water column of the along-estuary transect (Blanton et al. 1999). For this reason, an infinite bottom sediment pool was specified for both sand and settleable particles, which means that as long as bottom shear stress is larger than the critical shear stress for the resuspension of sand and settleable particles, then sand and settleable particles will be available in the bottom sediment pool for resuspension. No bottom sediment pool was specified for the nonsettleable particles (Table 1) since they are considered to be in permanent suspension in the water column.

The suspended sediment model was coupled with the Satilla River estuary 3-D hydrodynamic model developed in Zheng et al. (2003), which includes the flooding-drying cycle over intertidal salt marshes. The hydrodynamic model is driven by M_2 , S_2 , and N_2 tidal forcings at the open boundary over the inner shelf of the South Atlantic Bight and real-time freshwater discharge at the upstream end of the estuary. A detailed description of the design of the numerical experiments for tidal and salinity

simulation is given in Zheng et al. (2003). At first, the model was run with tidal forcing only. When tidal elevations and currents reached a quasi-equilibrium state, the tidal currents, surface elevation, and turbulent mixing coefficients at the time of neap tide slack low water were stored as an initial flow field for the coupled hydrodynamic and sediment model. Then the coupled model ran prognostically for an additional 9 d (until April 16, 1995) under the initial physical condition specified using the along-estuary distribution of salinity measured on April 7, 1995. A spatially uniform sediment concentration was specified as the initial condition for the sediment model. This is consistent with our interest in determining the extent to which the spatial structure of suspended sediment is driven by physical processes.

Model Results

The coupled model reasonably reproduced the along-estuary distribution of TSS observed in the Satilla River estuary in April 1995, as shown in Fig. 1. The model predicted a non-uniform distribution of TSS in an along-estuary transect, with two maxima near the bottom: one near the mouth of the estuary and the other 13 km upstream where the shoreline has a significant concave bend (Fig. 2). In these two maxima regions, TSS concentration has a large vertical gradient near the bottom and is uniform within 3 m of the surface. The TSS concentration has a maximum value of more than 250 mg l^{-1} near the bottom and a minimum value of about 20 mg l^{-1} near the surface. These locations of high TSS concentrations are the same as those found in the observations (Fig. 1).

The model-predicted temporal variation of TSS concentration was also in reasonable agreement with the data taken at an anchor station over one M_2 tidal cycle on April 16, 1995 (see Fig. 1 in Zheng et al. 2003 for the location and Figs. 1 and 2 for the model-data comparison). The model-predicted TSS concentration at that site varied periodically with the M_2 tidal cycle; it showed two maxima near the bottom 1 to 2 h after maximum ebb and flood currents and two minima at slack high water and slack low water, which is consistent with observations. During maximum flood and ebb tides, the TSS concentration in the model reached $1,000 \text{ mg l}^{-1}$ near the bottom and rapidly decreased upward to 100 mg l^{-1} near the surface. During slack waters, the TSS concentration in the water column was less than 100 mg l^{-1} .

At maximum flood and ebb tidal currents, the model-predicted TSS concentration near the bottom was about 30% sand and 70% settleable particles. The model also showed that upward resuspension was weaker during ebb tide than it was

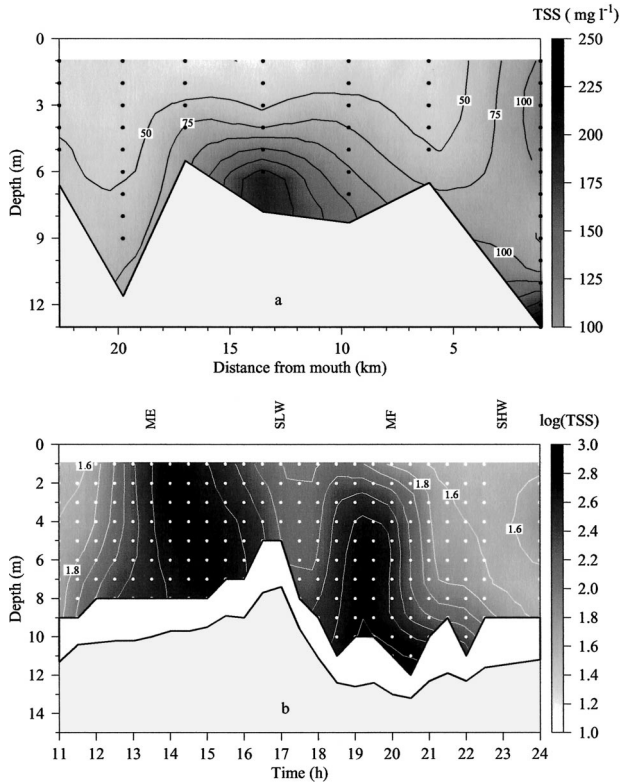


Fig. 1. The distributions of TSS observed along the estuary on April 15, 1995 (upper panel), and at an anchor site over a tidal cycle (lower panel) on April 16, 1995, in the Satilla River estuary (ME: maximum ebb, MF: maximum flood, SLW: slack low water, SHW: slack high water). Dots in the upper and lower panels represent measurement locations. During the measurement at the anchor station, the surface was selected as the origin of the coordinate ($z = 0$). The shaded area in the lower panel includes the temporal variation of sea elevation plus change of bottom depth due to the boat's shift.

during flood tide. These temporal distribution patterns were in reasonable agreement with the observations shown in Fig. 1. On the other hand, there were several differences between observational and model data in terms of spatial variations. First, model-predicted TSS concentrations near the bottom on the along-estuarine transect were about 50 mg l^{-1} higher than the observations (Figs. 1 and 2). This might be due to the vertical resolution of the measurements. Since observations were recorded 1.5–3 m above the bottom, they might have failed to resolve higher concentrations near the bottom. When we plotted model-predicted TSS concentrations at the same depth as the field observations, we obtained comparable TSS concentrations. Another difference between observational and model data occurred at the anchor site. Field observations showed significant asymmetry in TSS distribution over one M_2 tidal cycle, with a narrow peak in suspended sediment around maximum

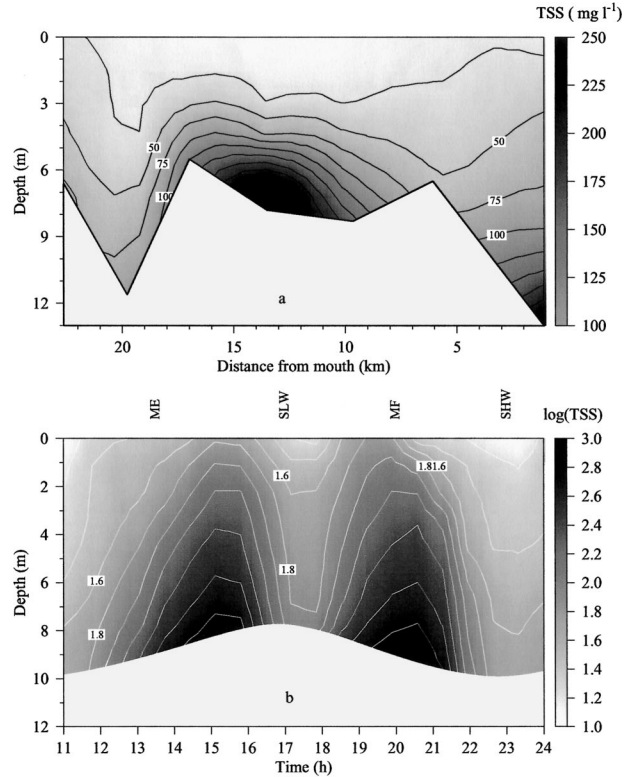


Fig. 2. The model-predicted distributions of TSS along the estuary on April 15, 1995 (upper panel), and at an anchor site over a tidal cycle (lower panel) on April 16, 1995, in the Satilla River estuary for the case with tidal forcing plus real-time freshwater discharge. Abbreviations as described for Fig. 1. To compare with the observation data shown in Fig. 1, the surface was selected as the origin of the coordinates in the lower panel, so the shaded area indicates the temporal variation of surface elevation.

flood tide and relatively high concentrations near the surface during both the ebb tidal phase and at slack low water. Neither of these differences was resolved in our coupled model simulation. These discrepancies were possibly the result of strong vertical mixing caused by the interaction of spring tide and surface wind, as well as outflow of suspended sediment from the intertidal salt marshes during ebb tide (Blanton et al. 1999). Since the model did not include surface wind forcing and processes associated with resuspension and sedimentation in the intertidal salt-marsh area, we did not expect good model-data comparison for these two features.

We used information on the different sediment fractions to explore the along-estuary distribution of model-predicted sand, settleable, and nonsettleable particles. The TSS was dominated by the settleable particles near the bottom and by nonsettleable particles in the upper water column. An example can be seen from the along-estuary distri-

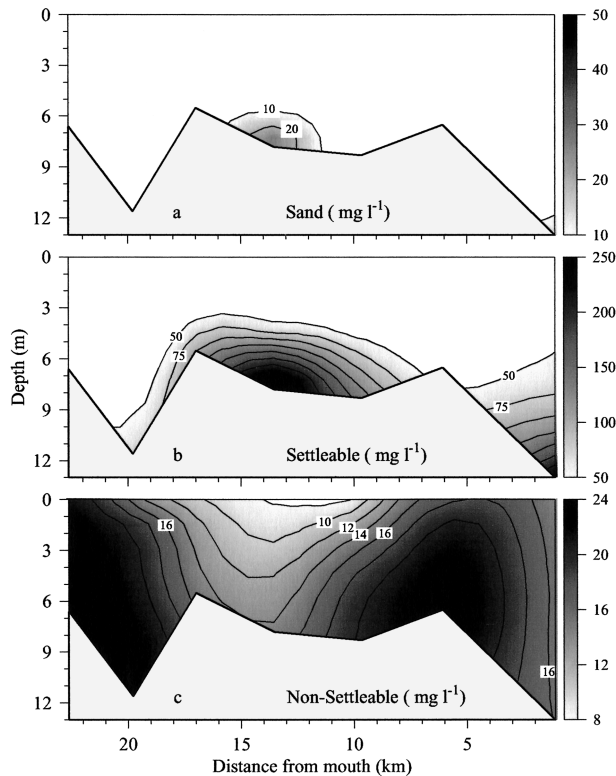


Fig. 3. Model-predicted, along-estuary distributions of (a) sand, (b) settleable particles, and (c) nonsettleable particles concentrations on April 15, 1995, for the case with tidal forcing plus real-time freshwater discharge.

bution of these three sediment fractions at slack high water (Fig. 3). The sand is trapped near the bottom and has a maximum concentration of about 20–30 mg l^{-1} . This amount of material only accounts for 10–15% of the total near-bottom sediment concentration (Fig. 3a). These low sand concentrations are likely due to its relatively fast settling velocity. With a settling velocity of 2.8 cm s^{-1} , no sand would be able to remain suspended in the water column longer than 5 min. The settleable particles are also trapped mainly near the bottom and exhibit two maxima of 200 mg l^{-1} or higher; one occurs near the mouth of the estuary and the other is 13 km upstream (Fig. 3b). The concentrations of sand and settleable particles near the surface are very small and can be neglected. The model-predicted nonsettleable particles dominated in the upper 3 m of the water column (Fig. 3c). Their concentration is only about 25 mg l^{-1} near the bottom and about 10 mg l^{-1} near the surface.

The nonsettleable fraction exhibited spatial variation along-estuary, with the highest concentrations occurring at 6 and 23 km upstream. It should be noted that these high concentrations are located in the regions of weaker vertical stratification

(Fig. 8 in Zheng et al. 2003), which is consistent with a previous study by Geyer (1993). Geyer (1993) demonstrated that when the settling velocity of sediment in stratified water is between 0.01 and 0.1 cm s^{-1} (intermediate-size such as nonsettleable particles), it can accumulate in the vertical stratification region where a bottom convergence zone exists. Smaller particles are almost permanently suspended in the water column and coarser particles (such as sand and settleable particles) can sink to the bottom quickly, so the effect of stratification on the spatial distributions of these smaller or coarser sediments becomes insignificant.

Mechanism Studies

Both the observations and model results presented here show that TSS is distributed non-uniformly along the Satilla River estuary, with highest concentrations occurring near the mouth of the estuary as well as near the bend located 13 km upstream. What are the physical driving mechanisms responsible for such a spatial distribution of TSS? Are all the physical processes associated with horizontal convergence and divergence, buoyancy-induced flow, shoreline curvature effects, asymmetrical tidal mixing, and the flooding-drying cycle over the intertidal salt marshes equally important or are some of these processes dominant? To address these questions, a model-guided mechanistic study was carried out by examining the roles of the individual physical forcings and vertical eddy viscosity in the spatial distribution of TSS. Three numerical experiments were conducted under specified conditions with no river discharge, constant vertical eddy viscosity, and no inclusion of the salt-marsh intertidal zone, respectively. In the first case, salinity was specified at a constant value of 35 psu throughout the model domain. In the second case, the vertical eddy viscosity was specified as $1.0 \times 10^{-2} \text{ m}^2 \text{ s}^{-1}$, which is equal to the tidally and spatially averaged value of the model-predicted vertical eddy viscosity coefficient from the Mellor and Yamada's (1982) level 2.5 turbulent closure model.

The model results show that removing freshwater discharge does not alter the along-estuary distribution pattern of TSS, i.e., two maxima near the bottom on the along-estuary transect. The concentration, however, becomes much smaller, with a TSS concentration of about 100 mg l^{-1} near the bottom as compared to 250 mg l^{-1} (Fig. 4 left panel). This suggests that freshwater discharge is not an essential physical factor that is responsible for the occurrence of these two TSS maxima at the near mouth of the estuary and a distance of 13 km upstream. The decrease in magnitude of TSS is due to the fact that in the absence of freshwater discharge-induced vertical stratification, the verti-

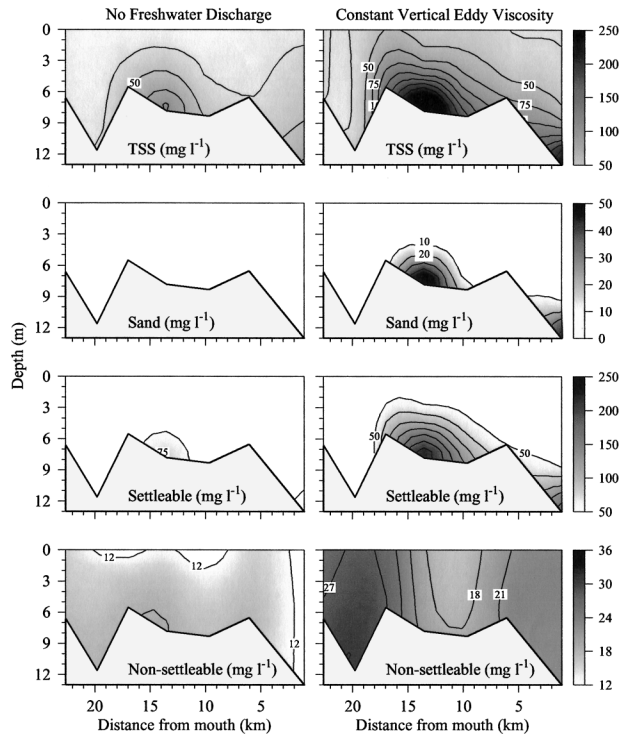


Fig. 4. Model-predicted, along-estuary distribution of total, sand, settleable particles, and nonsettleable particles concentrations on April 15, 1995, for the cases with no freshwater discharge and constant background salinity distribution (left panel) and constant vertical eddy viscosity (right panel).

cal shear of the horizontal current decreases dramatically. As a result, the bottom stress drops and less sediment can be resuspended from the bottom into the water column. When we look separately at the along-estuary distributions of sand, settleable, and nonsettleable particle fractions (Fig. 4 left panel), we see that the contribution of sand is extremely low and the TSS consists mostly of settleable particles near the bottom and of nonsettleable particles near the surface. The nonsettleable particles are distributed uniformly along the estuary with a value of about 10 mg l^{-1} . The fact that the two maxima of nonsettleable particles disappear under these conditions suggests that the spatial distribution of this type of sediment is effectively controlled by vertical stratification. This is, again, consistent with Geyer's (1993) finding that the temporal and spatial distributions of fine sediments in estuaries are closely associated with vertical stratification. It should be noted that the concentration of nonsettleable particles accounts for less than 5% of total TSS concentration near the bottom.

When the eddy viscosity coefficient was held constant during the model run, the model-predicted TSS again exhibited two maxima at the same locations as in the observations (Fig. 4 right panel).

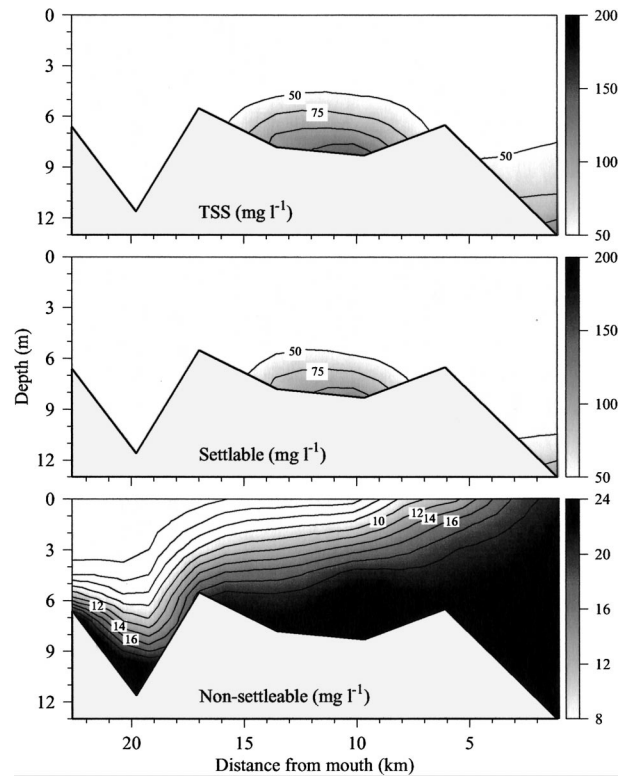


Fig. 5. Model-predicted, along-estuary distribution of total, settleable particles, and nonsettleable particles concentrations on April 15, 1995, for the case without inclusion of the flooding-drying process over intertidal salt marshes.

This implies that asymmetrical tidal mixing due to temporal and spatial variations of current shear is not an essential mechanism responsible for the observed spatial distribution of TSS in the Satilla River estuary. Individually, the distributions of sand and settleable particles are similar to those observed in the full model run, where we used variable vertical viscosity values predicted from the Mellor and Yamada's (1982) level 2.5 model (Figs. 3b,c and 4 right panel). However, the two maxima of nonsettleable particles observed near the bottom in the regions with relative strong vertical stratification disappear under this run, suggesting that asymmetric tidal mixing is more essential for nonsettleable particles than for settleable particles and sand.

Removing the flooding-drying cycle leads to a 30% reduction of TSS concentration. It also causes the location of the near-bottom maximum TSS concentration to shift downstream, so that it is located about 9 km upstream from the estuary as opposed to 13 km upstream (Fig. 5). Such a significant reduction of TSS is due to a significant underestimation of tidal currents and bottom shear stress in the case without inclusion of flood-

ing-drying cycle (Zheng et al. 2003). This results in a large decrease in the concentration of settleable particles (Figs. 3b and 5) and the disappearance of sand from the estuary. The nonsettleable particles are trapped in the lower water column under these conditions. This results from the fact that vertical mixing is significantly reduced and the settling process becomes relatively important when the flooding-drying cycle of the intertidal salt marshes is removed (Fig. 5). The shift in the location of the TSS maximum is a result of the relative importance of tidal and buoyancy flows. Freshwater discharge-induced buoyancy flow is one order of magnitude smaller than that of tidal currents. When tidal currents become weak under fixed lateral boundary conditions, this offshore buoyancy flow becomes relatively more important and drives the TSS downstream.

Discussion

The coupled 3-D hydrodynamic and suspended sediment model has reasonably reproduced the spatial and temporal distribution of TSS observed in the Satilla River estuary. Several model experiments have been conducted to examine the physical mechanism responsible for spatial and temporal distributions of TSS. These model experiments imply that neither asymmetric tidal mixing, freshwater discharge, nor the flooding-drying cycle over the intertidal salt marshes is the essential physical driving mechanism responsible for the two near-bottom TSS maxima observed near the mouth of the Satilla River estuary and 13 km upstream where the shoreline has a significant bend.

Previous study has revealed that the distributions of TSS in an estuary are closely related to estuarine circulation patterns (Festa and Hansen 1978). The hydrodynamic model (Zheng et al. 2003) predicted that residual currents in the estuary are characterized by multiple convergent and divergent circulation cells (Fig. 6). These complex residual flow patterns have been recently demonstrated using towed-ADCP measurements collected from the Satilla River estuary (Seim personal communication). The physical mechanisms responsible for the formation of these convergent and divergent flows are the buoyancy-induced along-estuary pressure gradient, bottom topographic tidal rectification, inertial curvature shoreline effects, and asymmetry of tidal currents associated with the flooding-drying cycle of intertidal salt marshes (Zheng et al. 2003). It is interesting to find that the two maximum TSS concentrations shown in Fig. 1 are located in a strong surface convergent flow zone (Fig. 6). In the surface-convergent flow, based on mass conservation there will be a downwelling zone that will enhance the sinking velocity of sus-

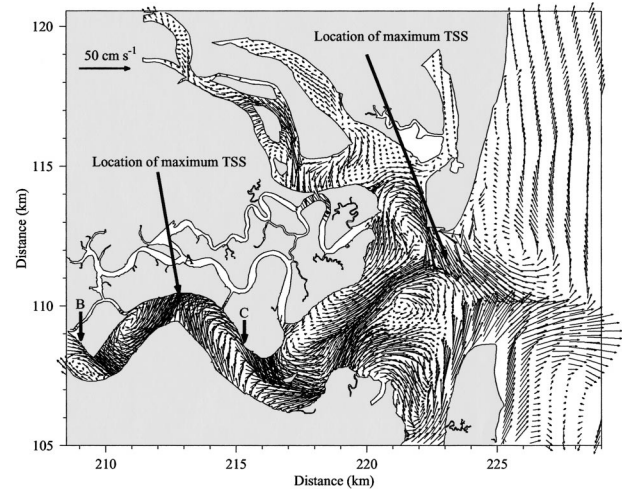


Fig. 6. Synoptic distribution of near-surface residual current vectors on April 15, 1995, for the case with tidal forcing plus real-time freshwater discharge. The location of maximum observed TSS is marked as site A. Two surrounding sites B and C are marked for comparisons of model results.

ended sediment. When suspended sediment is carried from the surrounding area to the convergent zone, it will quickly sink and deposit on the bottom due to its increased settling velocity. The horizontal convergence of the surface residual circulation is probably one of the mechanisms responsible for the formation of the two observed TSS maxima. This result is consistent with the findings by Jewell et al. (1993) on the Amazon continental shelf, where they found that the sediment accumulation rate or near-bottom suspended sediment concentration was largest in a zone of convergence.

More evidence for the idea that convergence patterns are important in determining TSS distribution can be seen in the cross-estuary distribution of residual vertical velocity at three selected sites (A, B, and C shown in Fig. 6). At site A, where the largest shoreline bend is located, the horizontally convergent flow near the surface causes a downward motion that hastens sinking of suspended sediment (Fig. 7a). At sites B and C, the horizontally divergent flow near the surface leads to a remarkable upward motion (upwelling zone) that cancels the settling velocity of suspended sediment and tends to carry material away from these two regions (Fig. 7b,c).

The model-predicted along-estuary distribution of TSS concentration is also likely related to the spatially non-uniform distribution of bottom stress, which is largest at site A and smaller at sites B and C (Fig. 8a,b). One of the most important sources for suspended sediment in the water column is the resuspension of bottom sediment. Equation 4 sug-

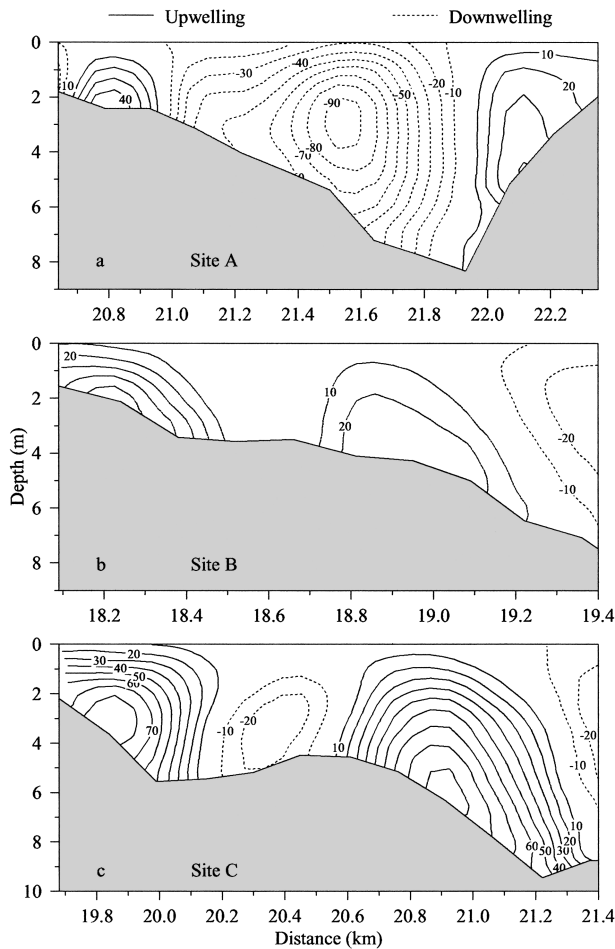


Fig. 7. Cross-estuary distribution of residual vertical velocity ($\times 10^{-3} \text{ cm s}^{-1}$) at three selected sites A, B, and C on April 15, 1995, for the case with tidal forcing plus real-time freshwater discharge. Filled triangles show the locations of field observations. The contour interval is $1 \times 10^{-2} \text{ cm s}^{-1}$.

gests that the amount of suspended sediment resuspension is proportional to the difference between bottom stress and critical shear stress for resuspension if bottom sediment is available. Our model results suggest that TSS near the bottom is dominated by settleable particles. Since the initial pool for this sediment fraction was given as infinite, the location of maximum TSS should be consistent with the place where the largest bottom shear is observed. Thus the maximum TSS concentration at 13 km upstream might be caused by surface convergence as well as significant bottom stress that results in more resuspension.

The asymmetric distribution of TSS concentration found in flood and ebb tides, i.e., a relatively weaker upward resuspension of the sediment in the water column (Fig. 2b) during ebb tidal phase compared to that during flood tidal phase, is clearly caused by asymmetrical tidal mixing over a tidal

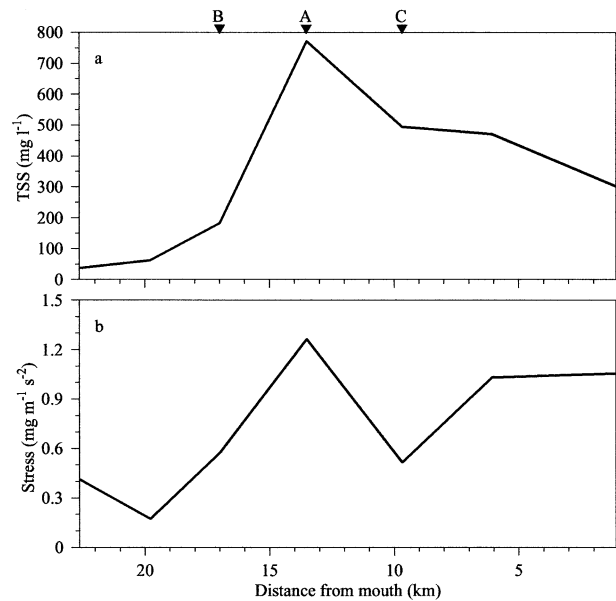


Fig. 8. Along-estuary distribution of depth-averaged TSS concentration (upper) and bottom stress (lower) averaged over an M_2 tidal cycle on April 15, 1995. Filled triangles show the locations of sites A, B, and C shown in Fig. 6.

cycle. The model-predicted vertical eddy viscosity is stronger during flood tidal phase, which suggests stronger vertical mixing (Fig. 9a). Weaker tidal mixing during ebb tidal phase is caused by the superimposition of gravitational and tidal flows, leading to a relatively large vertical stratification and a decrease of vertical mixing. A relatively stronger bottom current speed is found during flood tidal phase that leads to a larger bottom stress and more active upward sediment resuspension during this tidal phase (Fig. 9b).

The 1–2-h time lag for the occurrence of maximum TSS concentration relative to the maximum tidal current at ebb and flood tides is believed to be due to the fact that the bottom shear stress within 1 to 2 h after maximum current is still large enough to produce bottom sediment resuspension dominant over sedimentation. This results in net suspended sediment transport from bottom sediment. When it is at the stage that the amount of resuspension is the same as that of sedimentation, the TSS concentration reaches its maximum. After this point, the sedimentation process becomes dominant over the resuspension process, resulting in net sediment deposition and a decrease of TSS concentration. Due to a larger near-bottom velocity during the flood tidal phase, a longer time lag occurs during this period, which is consistent with both observations (Fig. 1b) and model results (Fig. 2b).

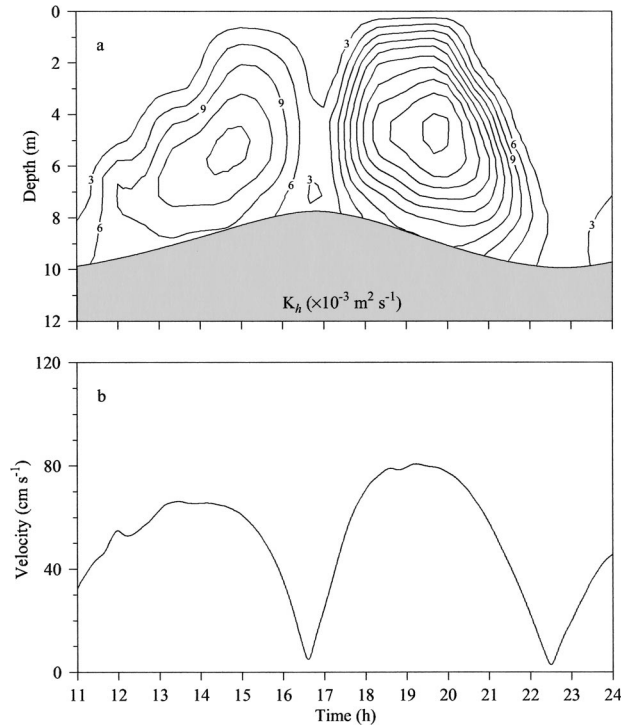


Fig. 9. Time sequence of the distribution of vertical eddy viscosity K_h ($\times 10^{-3} \text{ m}^2 \text{ s}^{-1}$) (upper panel) and bottom current speed (lower panel) over an M_2 tidal cycle on April 15, 1996 for the case with tidal forcing plus real-time freshwater discharge. The location of this plot was at the anchor site (see Fig. 1 in Zheng et al. 2003). The surface was selected as the origin of the vertical coordinate and the shaded area in the upper panel represent the temporal variation of surface elevation over a tidal cycle.

ACKNOWLEDGMENTS

This research was supported by the Georgia Sea Grant College Program under grant numbers NA26RG0373 and NA66RG0282 for Dr. Changsheng Chen, and by the National Science Foundation Land-Margin Ecosystems Research Program Grant No. DEB-9412089 for Dr. Meryll Alber. Dr. Lianyuan Zheng was supported by Dr. Chen's Sea Grant funds. We thank Dr. Jack Blanton of Skidaway Institute of Oceanography (SKIO) for providing the observational data used for validating the model. These observations were collected through support to SKIO provided by the Georgia Coastal Zone Management Program (Grant No. RR100-279/9262764), the National Science Foundation (LMER Grant No. DEB-9412089), (LTER Grant No. OCE-9982133), and a grant from the Georgia General Assembly. We thank Dr. Mac Rawson for his encouragement and help in project organization. We would like to thank Dr. Clark Alexander for permission to use his observed suspended sediment data. The 2-m elevation line was obtained from the GIS database created by Dr. Alice Chalmers; this work would be impossible without her kind help. We also want to thank Mr. George Davidson and anonymous reviewers for their editorial help.

LITERATURE CITED

ARIATHURAI, R. AND R. B. KRONE. 1976. Mathematical modeling of sediment transport in estuaries, p. 98–106. In M. Wiley (ed.), *Estuarine Processes*. Academic Press, New York.

- BLAKE, A. C., G. C. KINEKE, T. G. MILLIGAN, AND C. R. ALEXANDER. 2001. Sediment trapping and transport in the ACE basin, South Carolina. *Estuaries* 24:721–733.
- BLANTON, J., C. R. ALEXANDER, M. ALBER, AND G. KINEKE. 1999. The mobilization and deposition of mud deposits in a coastal plain estuary. *Limnologia* 29:293–300.
- DRONKERS, J. 1986. Tidal asymmetry and estuarine morphology. *Netherlands Journal of Sea Research* 20:117–131.
- DYER, K. R. 1986. *Coastal and Estuarine Sediment Dynamics*. John Wiley and Sons, New York.
- FESTA, J. F. AND D. V. HANSEN. 1978. Turbidity maxima in partially mixed estuaries: A two-dimensional numerical model. *Estuarine, Coastal and Shelf Science* 7:347–359.
- FISCHER, H. B., B. E. LIST, R. C. Y. KUO, J. IMBERGER, AND N. H. BROOKS. 1979. *Mixing in Inland and Coastal Waters*. Academic Press, New York.
- FITZGERALD, D. M. AND D. NUMMEDAL. 1983. Response characteristics of an ebb-dominated tidal inlet channel. *Journal of Sedimentary Petrology* 53:833–845.
- GEYER, W. 1993. The importance of suppression of turbulence by stratification on the estuarine turbidity maximum. *Estuaries* 16:113–125.
- JAY, A. J. AND J. D. MUSIAK. 1994. Particle trapping in estuarine tidal flows. *Journal of Geophysical Research* 99:445–461.
- JEWELL, P. W., R. F. STALLARD, AND G. L. MELLOR. 1993. Numerical studies of bottom shear stress and sediment distribution on the Amazon continental shelf. *Journal of Sedimentary Petrology* 63:734–745.
- LOU, J. AND P. V. RIDD. 1997. Modelling of suspended sediment transport in coastal areas under waves and currents. *Estuarine, Coastal and Shelf Science* 45:1–16.
- MELLOR, G. L. AND T. YAMADA. 1982. Development of a turbulence closure model for geophysical fluid problems. *Review of Geophysics* 20:851–875.
- MIDDLETON, G. V. 1976. Hydraulic interpretation of sand size distributions. *Journal of Geology* 84:405–426.
- POSTMA, H. 1967. Sediment transport and sedimentation in the estuarine environment, p. 158–179. In G. H. Lauff (ed.), *Estuaries*, American Association Advanced Scientific Publication 83. Washington, D.C.
- RIDD, P. V., T. STIEGLITZ, AND P. LARCOMBE. 1998. Density-driven secondary circulation in a tropical mangrove estuary. *Estuarine, Coastal and Shelf Science* 47:621–632.
- SANFORD, L. P., W. PANAGIOTOU, AND J. P. HALKA. 1991. Tidal resuspension of sediments in northern Chesapeake Bay. *Marine Geology* 97:87–103.
- UNCLES, R. J. AND J. A. STEPHENS. 1993. The freshwater-saltwater interface and its relationship to the turbidity maximum in the Tamar estuary, United Kingdom. *Estuaries* 16:126–141.
- ZHENG, L., C. CHEN, AND H. LIU. 2003. A modeling study of the Satilla River estuary, Georgia. Part I: Flooding-drying process and water exchange over the salt marsh-estuary-shelf complex. *Estuaries* 26:651–669.

SOURCES OF UNPUBLISHED MATERIALS

- ALEXANDER, C. Unpublished Data. Skidaway Institute of Oceanography, Savannah, Georgia 31411.
- SEIM, H. Personal Communication. Department of Marine Sciences, University of North Carolina, Chapel Hill, North Carolina 27599.

Received for consideration, December 1, 2000

Revised, June 5, 2002

Accepted for publication, July 9, 2002